symmetry

MDPI

Article

Study of Low-Frequency Sound Absorption Based on Negative Stiffness Membrane Structure

Xiaoyuan Zheng [1], Chenxu Fu [1], Hongbai Bai [1], Zhu Lin [2] and Xingxing Liu [1,*]

[1] School of Mechanical Engineering and Automation, Fuzhou University, Fuzhou 350116, China
[2] Guangdong Science & Technology Infrastructure Center, Guangdong Provincial Key Laboratory of High Performance Computing, Guangzhou 510033, China
* Correspondence: liuxingxing432@fzu.edu.cn

Abstract: The system stiffness of a negative stiffness membrane structure is widely investigated in metamaterial research, and some special performances have been achieved. While for acoustics, low-frequency absorption still remains a big issue, so in this work, a negative stiffness membrane structure with its theoretical calculation model and experimental verification of sound absorption is established. Moreover, the nonlinear stiffness changes of the thin film under different deformation conditions and different spacing between two permanent magnets are systematically analyzed, obtaining the theoretical stiffness analytical equation of the negative stiffness thin-film structure system. Combined with finite element simulation analysis, the stiffness variation rule and influencing factors of the negative stiffness membrane system are discussed. Specifically, the impact of the mass radius, mass thickness, and film thickness on the magnetic force and system stiffness is analyzed. Based on the acquired testing results, the proper addition of the magnetic suction structure will induce a shift of the absorption peak to a lower frequency region. This work provides useful insights for the further development of the low-frequency sound absorption theory and testing prototype with a negative stiffness membrane structure.

Keywords: thin film acoustic metamaterial; negative magnetic stiffness; magnetic-solid coupling; acoustic-solid coupling; low-frequency sound absorption

Citation: Zheng, X.; Fu, C.; Bai, H.; Lin, Z.; Liu, X. Study of Low-Frequency Sound Absorption Based on Negative Stiffness Membrane Structure. *Symmetry* **2022**, *14*, 1858. https://doi.org/10.3390/sym14091858

Academic Editor: Sergei Alexandrov

Received: 1 August 2022
Accepted: 31 August 2022
Published: 6 September 2022

1. Introduction

Nowadays, the majority of mature noise reduction methods are generally aimed at solving high-frequency noise, while the effect of reducing low-frequency noise is not satisfactory [1]. From the perspective of the acoustic theory, it is clear that the issue of low-frequency noise is difficult to be solved due to its long wavelength and high penetrability characteristics. However, the traditional design method needs to increase the thickness of the resistive sound-absorbing material or increase the back cavity depth of the resonator structure, which limits its practical applications. Acoustic metamaterials have been extensively studied in recent years and have provided some new ideas to solve these problems [2,3].

For the development of acoustic attenuation metamaterials, Li et al. [4] proposed the concept of acoustic metamaterial for the first time in 2004 and proposed a new type of phononic crystal and found that the direct control in the form of acoustic propagation can be attained. Such composite materials are defined as acoustic metamaterial (AM). Interestingly, sound-absorbing AM can absorb low-frequency sound waves with a relatively small size. They are mainly divided into the following categories: thin-film AM, thin plate AM and Helmholtz-based AM [5–9]. Among them, the thin film AM is mainly composed of polymer films and mass blocks, which consume energy through the vibration of the mass blocks. Yang et al. [10] proposed an AM with a thin film structure and found that it has a good sound insulation effect in the low-frequency range. Naify et al. [11] designed a new type of thin-film AM and found that the peak frequency of the sound absorption can be adjusted by changing the quality characteristics of the thin film. Mei et al. [12] embedded asymmetric semi-circular metal sheets on the surface of the film, and by carrying out experiments and simulation analysis, it is concluded that the structure can effectively absorb sound waves in the low-frequency band (100–1000 Hz). Fan et al. [13] combined the film and the micro-perforated plate to achieve low-frequency sound insulation properties. Chen et al. [14] proposed a new type of AM based on petals and found that the acoustic band gap produced by this structure has more advantages than the traditional structure. In another interesting work, Gao et al. [15] designed a new type of double-layer membrane acoustic metamaterial, which controls the pre-stress of the membrane through the application of magnetic force. This method can control the vibration pattern of the structure and change the sound absorption characteristics. Langfeldt et al. [16] studied the bending stiffness of an additional mass and the acoustic coupling between elements, and an analytical model for this problem is established. In addition, the impacts of film pre-stress, mass, and asymmetric mass on the sound absorption performance of the structure are systematically studied. Sam et al. [17] fabricated a one-dimensional AM with effective negative density using an array of very thin elastic membranes, which exhibits effective negative density in a wide frequency range from 0 to 735 Hz. Kumar et al. [18] report a double negative AM for absorption of low-frequency acoustic emissions in an aircraft. And an average transmission loss of 56 dB under 500 Hz and overall absorption of over 48% have been realized experimentally. Yang et al. [19] proved that thin membrane-type AM could serve as a total reflection nodal surface at certain frequencies. Shen et al. [20] reported a broadband acoustic hyperbolic metamaterial using the two-dimensional unidirectional membrane array, and the proposed metamaterial could open up new possibilities for acoustic wave manipulation. Christiansen et al. [21] realized acoustic hyperbolic metamaterial through topology optimization and verified the predicted refractive capability as well as the predicted transmission at an interface.

The sound absorption effect of the thin-film AM has made a breakthrough in the low-frequency region. However, due to the stiffness of the structure, its sound absorption frequency band is difficult to continue to expand downward. Thus, it is not feasible to meet the existing sound absorption requirements [22,23]. Therefore, the design principle of negative stiffness is adopted in this work to reduce the stiffness of the structure to decrease the sound absorption frequency and improve the sound absorption effect meanwhile [24]. At present, few studies can be found about the negative stiffness properties of thin-film acoustic metamaterials, and only theoretical demonstrations and simple experiments have been carried out. However, the stiffness changes and various influencing factors of the whole structure of thin-film metamaterials by the introduction of negative stiffness, as well as the changes in the sound absorption performance caused by the negative stiffness, have not been deeply studied yet.

Along these lines, in this work, the thin-film acoustic metamaterial structure of a negative stiffness is analyzed, and its influencing factors and changing rules, as well as the influence of the final model on the sound absorption effect, are studied. The main purpose of this work is to explore the influence of different structural parameters on the overall stiffness of the system by performing theoretical stiffness modeling and finite element simulation analysis of the thin film and magnetic structures and designs appropriate negative stiffnesses of film type metamaterial achieving good sound absorption performance in the low-frequency range. This work has certain application merits and guiding values for the investigation of the system negative stiffness of thin-film acoustic metamaterials for sound attenuation.

This work is divided into three sections: First, the system stiffness of negative stiffness film structure is analyzed, and the sound absorption model of negative stiffness film is established. Second, COMSOL is used for simulation analysis to explore the relationship between the overall stiffness and displacement of the system under different parameters. Third, the experimental validation of the developed model is described, and the magnetic force test and sound absorption test have also been detailed.

2. Model Establishment

2.1. System Stiffness Analysis of Membrane Structures with Negative Stiffness

In order to decrease the sound absorption frequency, reducing the system stiffness is considered an important scheme for the thin-film sound absorption structure within the limitations of a certain size and structure. However, to reduce the overall stiffness of the system without changing the size of the original absorption cavity, it is necessary to introduce a negative stiffness structure realized by magnetic structure, which can effectively avoid the change of the sound absorption cavity. Therefore, the film-type sound absorption structure with negative stiffness properties has obvious advantages under the same size. In this work, the permanent magnet is used to realize the negative stiffness of the structure. As is shown in Figure 1a, a ferromagnetic mass block is placed in the center of the circular film, and a cylindrical permanent magnet is arranged at the bottom of the sound-absorbing cavity. In contrast, the permanent magnet is set below the mass block. Figure 1b illustrates the stress analysis diagram of the magnetic attraction structure. It is noteworthy that a nonlinear attraction between the mass P and the permanent magnet C will be developed [24]. Equation (1) shows the polynomial fitting relation between the magnetic force and displacement.

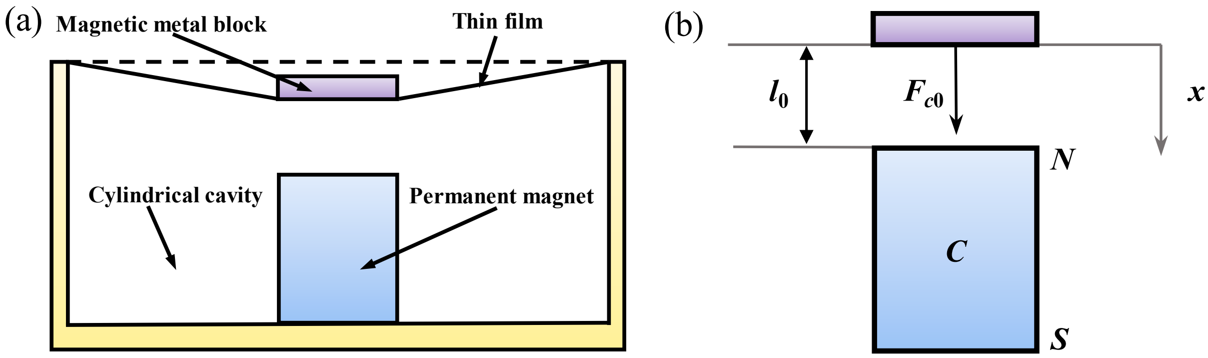

Figure 1. (**a**) Schematic diagram of the negative stiffness film structure and (**b**) stress analysis of the magnetic attraction structure.

$$F_c = -\left(F_{c0} + a_1 l + a_2 l^2 + a_3 l^3 + a_4 l^4\right) \quad (1)$$

where F_c is the magnetic force, F_{c0} represents the magnetic force when the two magnets are at the initial distance, l is the distance between the two magnets, and a_0~a_4 stands for the fitting parameters. Let $l = l_0 - x$ and substitute it into Equation (1) to obtain:

$$F_c = -\left(F_{c1} + b_1 x + b_2 x^2 + b_3 x^3 + b_4 x^4\right) \quad (2)$$

where:

$$\begin{aligned} F_{c1} &= -\left(F_{c0} + a_1 l_0 + a_2 {l_0}^2 + a_3 {l_0}^3 + a_4 {l_0}^4\right) \\ b_1 &= a_1 + 2a_2 l_0 + 3a_3 {l_0}^2 + 4a_4 {l_0}^3 \\ b_2 &= -\left(a_2 + 3a_3 l_0 + 6a_4 {l_0}^2\right) \\ b_3 &= a_3 + 4a_4 l_0 \\ b_4 &= -a_4 \end{aligned} \quad (3)$$

By deriving Equation (2), the negative stiffness of the magnetic force k_c can be obtained as follows:

$$k_c = -\left(b_1 + 2b_2 x + 3b_3 x^2 + 4b_4 x^3\right) \quad (4)$$

As shown in Figure 1, the system stiffness consists of the nonlinear positive stiffness k_n of the film and the nonlinear negative stiffness k_c between the permanent magnets. From the stress analysis shown in Figure 2, it can be seen that the displacement ω generated by the film is equal to the displacement change x of the two magnets, which can be used as a displacement variable in the system. Therefore, according to the superposition principle of the series structure, the system stiffness k can be obtained as follows:

$$k = k_n + k_c \tag{5}$$

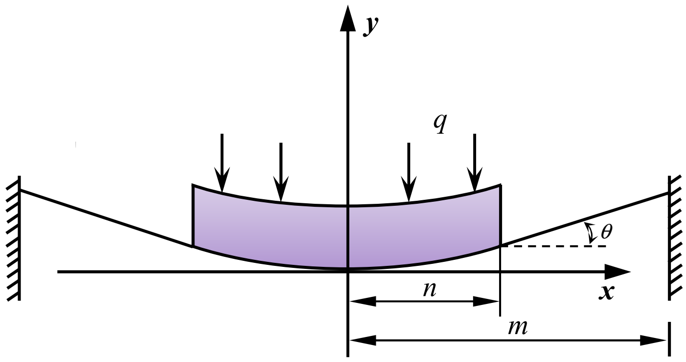

Figure 2. Stress analysis of the negative stiffness membrane structure.

For the thin film structure, when the value of φ at x = 1 is regarded as φ_1, and the value of φ at $x = \alpha^2$ is regarded as φ_a. Hence, it can be obtained [25]:

$$W = -\left(\frac{Qc}{2}\right)^{1/3} g(ca^2)\cdot a^2 + \left(\frac{Q\alpha^4}{2}\right)^{1/3}\left[\left(c\alpha^2\right)^{1/3} g\left(c\alpha^2\right) - \frac{2}{\sqrt{M}}(\varphi_\alpha - \varphi_1)\right] \tag{6}$$

where $Q = m^4 q/\delta^4 E, W = w/\delta, \alpha^2 = n^2/m^2$: M is the function of ca^2, q is the load, δ is the thickness of the film and c denotes the integral constant, and:

$$g(x) = 1 + \frac{1}{4}x + \frac{5}{36}x^2 + \frac{55}{576}x^3 + \frac{7}{96}x^4 + \frac{205}{3456}x^5 + \frac{17051}{338688}x^6 + \ldots\ldots \tag{7}$$

Therefore:

$$\frac{x}{\delta} = -\left(\frac{m^4 qc}{2\delta^4 E}\right)^{1/3} g(c\alpha^2)\cdot\alpha^2 + \left(\frac{m^4 q\alpha^4}{2\delta^4 E}\right)^{1/3}\left[\left(c\alpha^2\right)^{1/3} g\left(c\alpha^2\right) - \frac{2}{\sqrt{M}}(\varphi_\alpha - \varphi_1)\right] \tag{8}$$

It can be seen that the relationship between the uniformly distributed load q and the stress F_n of the film is the following:

$$F_n = \pi\alpha^2 m^2 q \tag{9}$$

Simultaneous from Equations (8) and (9) it can be obtained:

$$F_n = \frac{x^3}{\delta^3\left[\left(\frac{\alpha^2 m^2}{2\delta^4 E}\right)^{1/3}\left[(c\alpha^2)^{1/3} g(c\alpha^2) - \frac{2}{\sqrt{M}}(\varphi_\alpha - \varphi_1)\right] - \left(\frac{cm^2}{2\pi\alpha^2\delta^4 E}\right)^{1/3} g(c\alpha^2)\cdot\alpha^2\right]} \tag{10}$$

The positive stiffness of the membrane k_n can be obtained by the derivation of both sides of Equation (2):

$$k_n = 3b_0 x^2 \tag{11}$$

where:

$$b_0 = \frac{1}{\delta^3\left[\left(\frac{\alpha^2 m^2}{2\delta^4 E}\right)^{1/3}\left[(c\alpha^2)^{1/3} g(c\alpha^2) - \frac{2}{\sqrt{M}}(\varphi_\alpha - \varphi_1)\right] - \left(\frac{cm^2}{2\pi\alpha^2\delta^4 E}\right)^{1/3} g(c\alpha^2)\cdot\alpha^2\right]} \tag{12}$$

Simultaneous from Equations (4), (5) and (11) it can be obtained:

$$k = -b_1 - 2b_2x + 3(b_0 - b_3)x^2 - 4b_4x^3 \tag{13}$$

2.2. Theoretical Modeling of the Sound Absorption Characteristics

The proposed negative stiffness film structure is composed of the film mass block, the back cavity, and the magnetic attraction structure, as shown in Figure 3. Therefore, the total acoustic impedance expression also includes the acoustic impedance Z_M of the film mass block, the acoustic impedance Z_D of the cavity part, and the acoustic impedance change Z_n, which is caused by the magnetic attraction force:

$$Z = Z_M + Z_D + Z_n \tag{14}$$

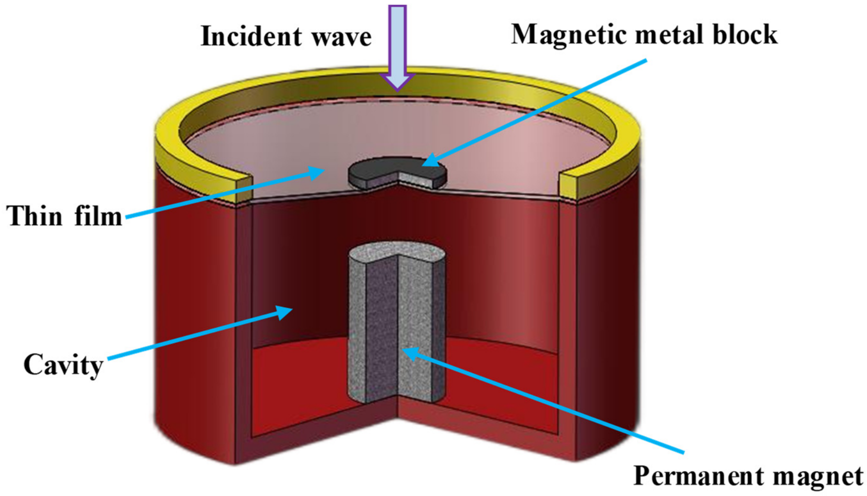

Figure 3. Three-dimensional schematic diagram of the negative stiffness membrane structure.

The expressions of the acoustic impedance Z_M, Z_D, and Z_n are as follows:

$$\left.\begin{array}{r} Z_M = R + Z_m \\ Z_D = -j\cot\left(\frac{\omega D}{c_0}\right) \\ Z_n = -j\frac{k}{\omega} \\ Z_m = j\omega\rho_1 \end{array}\right\} \tag{15}$$

where R is the sound resistance of the film material, k_D represents the air stiffness of the back cavity, ω is the angular frequency, k stands for the system stiffness of the film structure with negative stiffness, and ρ_1 denotes the density of the film material.

By the polynomial expansion of $\cot(\omega D/c_0)$, it can be obtained that the primary term is $c_0/\omega D$. Thus, Z_D can be approximately written as $Z_D = -jk_D/\omega$, where $k_D = c_0/D$. If the imaginary part of the acoustic impedance Z is zero, then the resonance frequency of the negative stiffness sound absorption structure can be obtained as follows:

$$f = \frac{1}{2\pi}\sqrt{\left(\frac{k_D + k}{m}\right)\rho_0 c_0} \tag{16}$$

Due to the addition of the magnetic absorption structure to the negative stiffness sound absorption structure, the nonlinear stiffness of the original film is changed. As a result, a new system stiffness k is formed, and the system's stiffness k will be reduced, Therefore, the resonance frequency will be moved to the low-frequency direction to achieve the shift of the sound absorption peak of the sound absorption structure to a lower frequency. As k decreases, the resonance frequency f will further decrease. Moreover, due to the magnetic absorption characteristics, the mass block at the balance position will start to oscillate, resulting in bigger amplitude oscillation and enhancing energy consumption. Therefore, the low-frequency sound absorption performance can also be improved to a certain extent.

The relative acoustic impedance Z' can be obtained by simultaneous use of Equations (14) and (15):

$$Z' = \frac{Z_M}{\rho_0 c_0} + Z_D + Z_n = R' + j\left(\frac{\omega m}{\rho_0 c_0} - \frac{k_D + k}{\omega}\right) \tag{17}$$

where $R' = R/\rho_0 c_0$ and according to the acoustic impedance method, the sound absorption coefficient expression of the negative stiffness sound absorption structure can be obtained as follows [22]:

$$\alpha = \frac{4\text{Re}(Z')}{[1 + \text{Re}(Z')]^2 + \text{Im}(Z')^2} = \frac{4\text{Re}(Z)\rho_0 c_0}{[\rho_0 c_0 + \text{Re}(Z)]^2 + \text{Im}(Z)^2} \tag{18}$$

where Re is the real part and Im is the imaginary part. In addition, when the imaginary part of the acoustic impedance Z is zero, the sound absorption coefficient α reaches the maximum value. At this time, the peak value of the sound absorption peak at the resonance frequency is $\alpha_{\max} = 4r'/(1 + r')^2$.

3. Magnetic Field Simulation Analysis of Negative Stiffness Membrane Structure

Due to the limitation of the theoretical analysis method for studying the influence of the magnetic attraction structure parameters on the magnetic field, numerical calculations with COMSOL are employed in this work to simulate variables of the radius and thickness of the mass block, the thickness of the permanent magnet, and the distance between the mass block and permanent magnet. Thus, the relationship between the force and displacement of the magnetic attraction structure under different parameters is systematically explored. Furthermore, the membrane structure is added to the finite element model to form the magnetic structure coupling finite element model. At the same time, the relationship between the overall stiffness and displacement of the system by considering different parameters is also examined.

3.1. Finite Element Analysis Method of Static Magnetic Field

For magnetostatic problems without current flow, the force in the magnetic field can be calculated by using the scalar magnetic potential:

$$\nabla \times \boldsymbol{H} = 0 \tag{19}$$

The magnetic scalar V_m can be defined as follows:

$$\boldsymbol{H} = -\nabla V_m \tag{20}$$

where $\boldsymbol{H}$ is the magnetic field strength, and ∇ represents the Hamiltonian operator that can be expressed as follows:

$$\nabla = e_x \frac{\partial}{\partial x} + e_y \frac{\partial}{\partial y} + e_z \frac{\partial}{\partial z} \tag{21}$$

The relationship between the magnetic flux density and the magnetic field is as follows:

$$\boldsymbol{B} = \mu_0(\boldsymbol{H} + \boldsymbol{M}) \tag{22}$$

where $\boldsymbol{B}$ is the magnetic induction intensity, $\boldsymbol{M}$ is the magnetization intensity, μ_0 stands for the permeability of the magnetic medium and:

$$\nabla \cdot \boldsymbol{B} = 0 \tag{23}$$

By combining Equations (20)–(23), the following expression can be obtained:

$$-\nabla\cdot(\mu_0\nabla V_{\mathrm{m}}-\mu_0\boldsymbol{M}_0)=0 \tag{24}$$

The magnetic field is tangent to the boundary in the plane of the symmetry, so it can be well described by the magnetic insulation conditions:

$$\boldsymbol{n}\cdot(\mu_0\nabla V_{\mathrm{m}}-\mu_0\boldsymbol{M}_0)=\boldsymbol{n}\cdot\boldsymbol{B}=0 \tag{25}$$

where $\boldsymbol{n}$ is the normal vector of the boundary. The force on the mass block is calculated by integrating the surface stress tensor on all the boundaries of the mass block. The following expression of stress tensor is used:

$$\boldsymbol{n}_1T=-\frac{1}{2}(\boldsymbol{H}\cdot\boldsymbol{B})\boldsymbol{n}_1+(\boldsymbol{n}_1\cdot\boldsymbol{H})\boldsymbol{B}^T \tag{26}$$

where $\boldsymbol{n}_1$ is the normal vector of the mass block pointing to the outside, and T denotes the stress tensor of the air. The force on the mass block can be obtained by integrating the above equation as follows:

$$F=\int_{\partial\Omega}\boldsymbol{n}TdS \tag{27}$$

3.2. Simulation Analysis of the Stiffness of the Magnetic Structure

The magnetic field finite element model of the magnetic attraction structure includes the dielectric domain, the mass block, and the permanent magnet. A schematic illustration of the finite element simulation model of the static magnetic field is shown in Figure 4. Obviously, the employed model in Figure 4a is symmetrical, so only one-quarter of the structure is intercepted during the modeling. On top of that, all bodies are divided by tetrahedral elements and free meshes. The XZ plane, YZ plane, and other boundaries of the peripheral dielectric domain are set as the magnetic insulation surface and the upper surface of the permanent magnet as the zero magnetic scalar potential surface. During the process of the simulation, the calculation of the surface stress tensor has to be calculated on all boundaries of the mass block and then integrated to complete the simulation calculation of the force on the mass block. Table 1 presents the geometric structure parameters of the proposed finite element simulation model of the magnetic attraction structure.

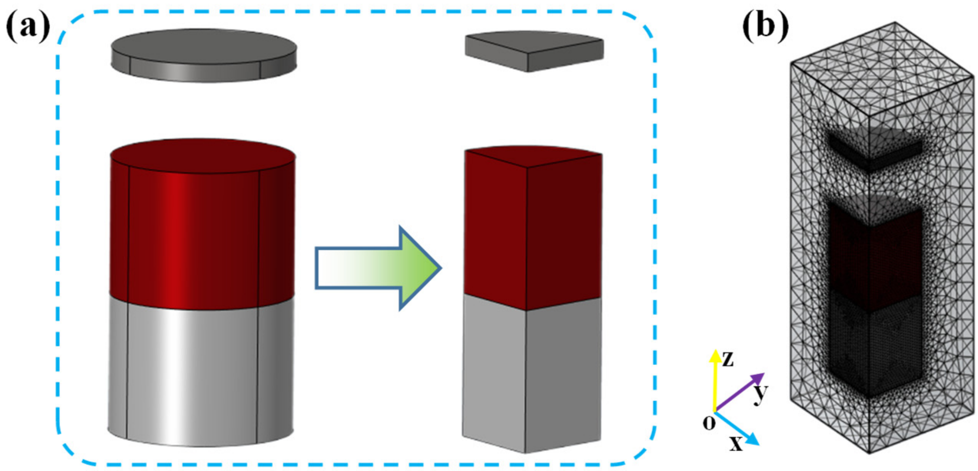

Figure 4. (**a**) Finite element simulation model diagram of the static magnetic field and (**b**) meshing of the static magnetic field finite element model.

Table 1. Calculation parameters of the magnetic attraction structure model.

Parameters	Radius of Mass Block (r)	Thickness of Mass Block (d)	Radius of Permanent Magnet (R)	Thickness of Permanent Magnet (H)
Values (mm)	10.0	2.0	10.0	30.0

3.2.1. The Influence on the Radius of the Mass Block

As shown in Figure 5, the magnetic force and magnetic stiffness increase obviously with the increase of the mass radius. Moreover, as increasing rates of different magnetic force and stiffness curves are getting larger, the impact of the increasing radius of the mass block on the enhancement of the magnetic force and magnetic stiffness is not significantly affected. The test device adopts an automatic guide rail slider, which can accurately locate the initial position of the slider and input a determined moving speed. Meanwhile, a high-precision laser sensor is used, which can accurately collect the displacement data of the magnet and the force sensor to obtain the test data accurately and quickly.

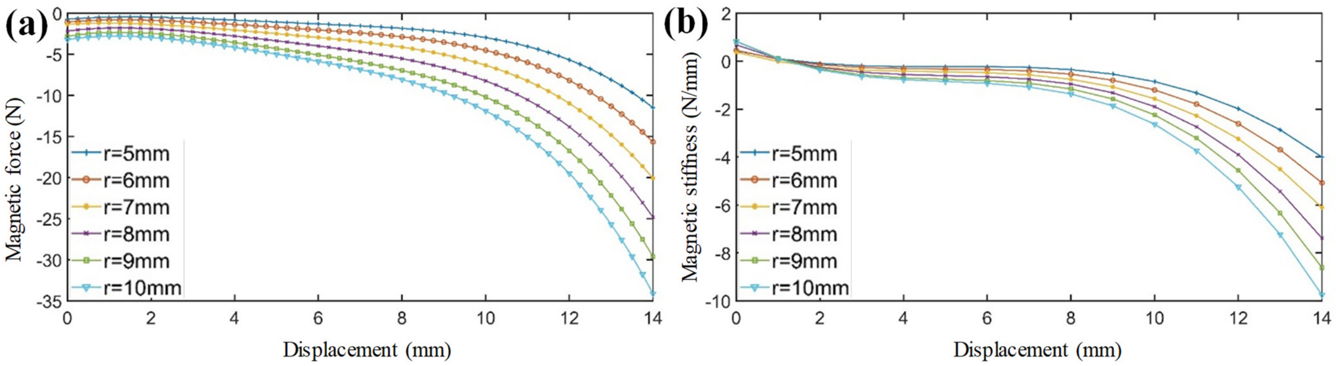

Figure 5. The influence on the radius of the mass block; (**a**) magnetic force, (**b**) magnetic stiffness.

3.2.2. The Influence on the Thickness of the Mass Block

The other parameters of the magnetic attraction structure remain unchanged according to Table 1, and only the thickness of the mass block is changed. Figure 6 shows the effect of the magnetic force and magnetic stiffness when the radius is increased from 0.5 mm to 3 mm. As shown in Figure 6, when the thickness of the mass block is increased, the magnetic force and magnetic stiffness are enhanced, obviously. Although the increasing rates are larger, it is found that the impact of the increased thickness of the mass block on the enhancement of the magnetic force and magnetic stiffness is gradually weakened.

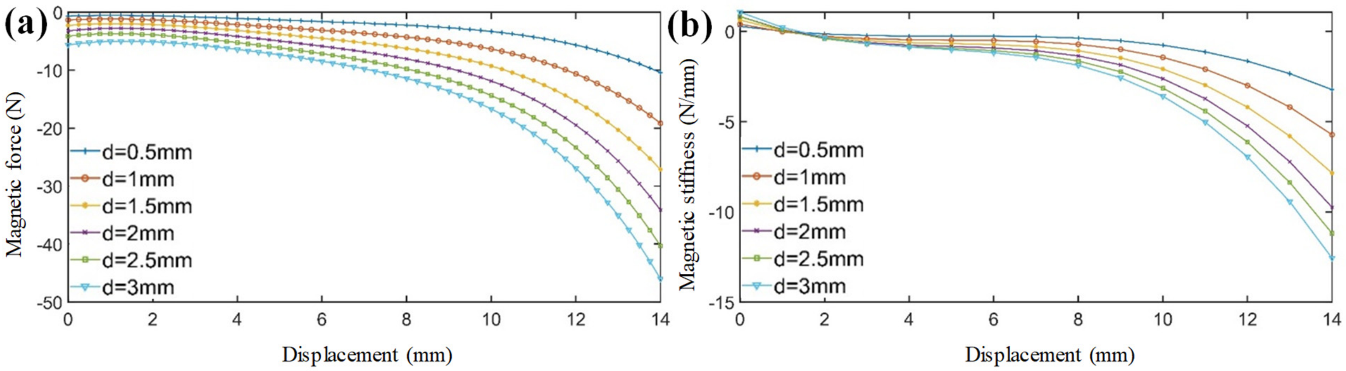

Figure 6. The influence on the thickness of the mass block; (**a**) magnetic force, (**b**) magnetic stiffness.

3.2.3. The Influence on the Thickness of the Permanent Magnet

Figure 7 displays the impact on the magnetic force and magnetic stiffness when the thickness of the permanent magnet is increased from 10 mm to 30 mm. As is shown in Figure 7, when the thickness of the permanent magnets increases, the magnetic force and magnetic stiffness do not change significantly. Therefore, the influence of the permanent magnet thickness on the magnetic force can be ignored in subsequent tests.

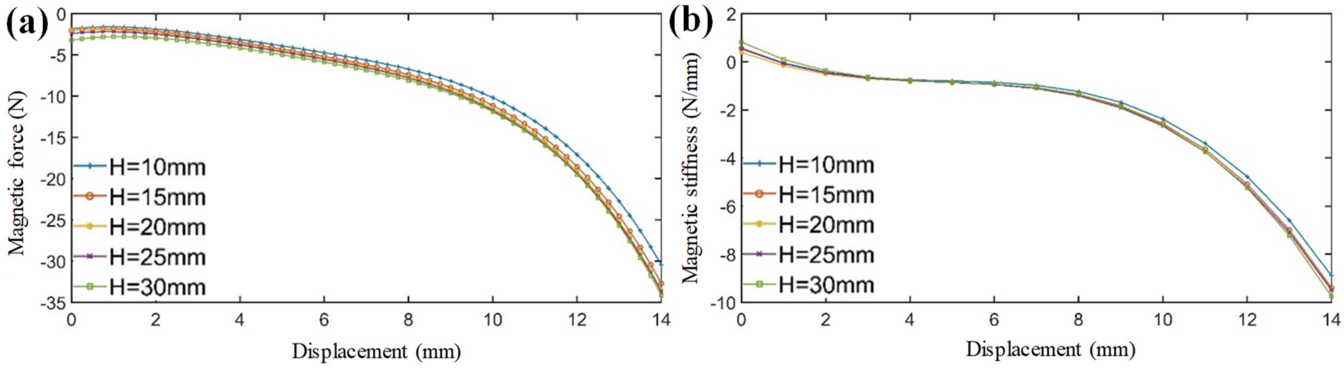

Figure 7. The influence on the thickness of the permanent magnet; (**a**) magnetic force, (**b**) magnetic stiffness.

3.3. Simulation Analysis of the Magnetic Structure-Coupling Field

The magnetic-solid coupling finite element model of the negative stiffness thin-film structure is incorporated into the thin-film frame of the magnetic attraction structure and its finite element model are shown in Figure 8.

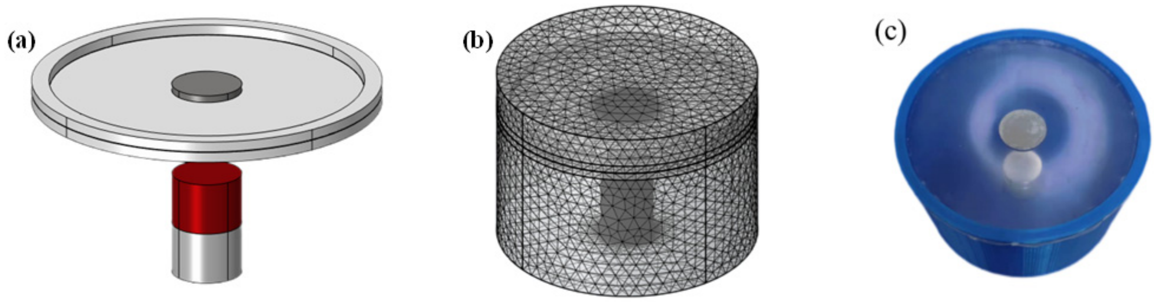

Figure 8. (**a**) Finite element simulation model diagram of the magnetic-solid coupling and (**b**) meshing of the magnetic-solid coupling finite element model, (**c**) manufactured testing sample.

For multi-physical field coupling, the magnetic field and the physical field of solid mechanics must be added first. Therefore, the thin film structure is added based on the three-dimensional model of the original magnetic attraction structure. In addition, it should be noted that the proposed simplified model couldn't be used for the simulation of the overall negative stiffness membrane structure because the model does not apply if the membrane structure cannot be subjected to complete edge fixed constraints. After the three-dimensional model is established, materials are added to it, and the magnetic absorption structure remains unchanged. The film material is made of pet-based material. The density of the material is 1200 kg/m^3, Young's modulus is 200 MPa, Poisson's ratio is 0.3, and the relative permeability is 1. When the structure is added to the corresponding physical field, the respective boundary conditions of the original magnetic attraction structure remain unchanged as the thin-film structure is added to the physical field of solid mechanics. The film is divided by sweeping the mesh, as shown in Figure 8b, and the manufactured testing sample is shown in Figure 8c. In the simulation model, various geometric parameters of the negative stiffness film structure are set according to Table 1, whereas the film radius is 45 mm and the film thickness is 0.2 mm.

The influence of the negative stiffness film structure on the system stiffness mainly includes the influence of the mass block radius, mass block thickness, and film thickness. For example, Figure 9a depicts the influence curve of the system stiffness when only the radius of the mass block is changed (5 mm to 10 mm). At the same time, other parameters remain unchanged, according to Table 1 Figure 9b shows the influence curve when only by changing the thickness of the mass block (0.5 mm–3 mm), and Figure 9c shows the results by only changing the thickness of the film (0.2 mm–1 mm).

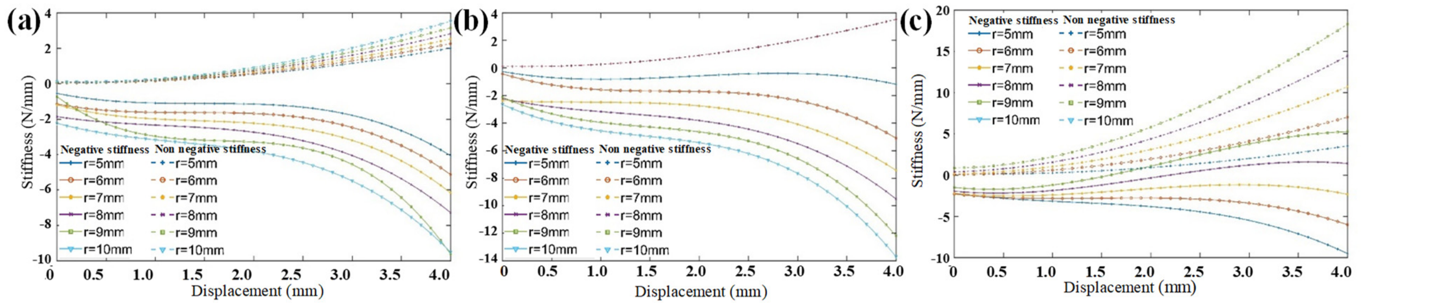

Figure 9. Impact of the parameters on the magnetic stiffness; (**a**) radius of mass block, (**b**) thickness of mass block, (**c**) thickness of the thin film.

As shown in Figure 9, the addition of the negative stiffness structure significantly reduces the stiffness of the system. Specifically, Figure 9a shows that when the radius of the mass block is increased, the system stiffness of the negative stiffness structure is gradually decreased. In contrast, the system stiffness of the non-negative stiffness structure is changed slightly. As shown in Figure 9b, when the thickness of the mass is increased, the stiffness of the system will be gradually decreased. However, it is found that the impact on the decreased stiffness of the system will be gradually weakened with the increase of the thickness. Additionally, in Figure 9c, when the film thickness is reduced, the system stiffness will also be significantly reduced. In contrast, the influence of the reduced stiffness will not be significantly affected by the reduction of the thickness.

4. Experimental Verification

4.1. Magnetic Force Test

The magnetic force test system of the negative stiffness thin-film structure is shown in Figure 10, whereas the model of the data collector is 3560D. The main components of the magnetic force testing device are the following: mounting base, automatic guide rail, laser displacement sensor (CD22-35), and force sensor (DLLF-88).

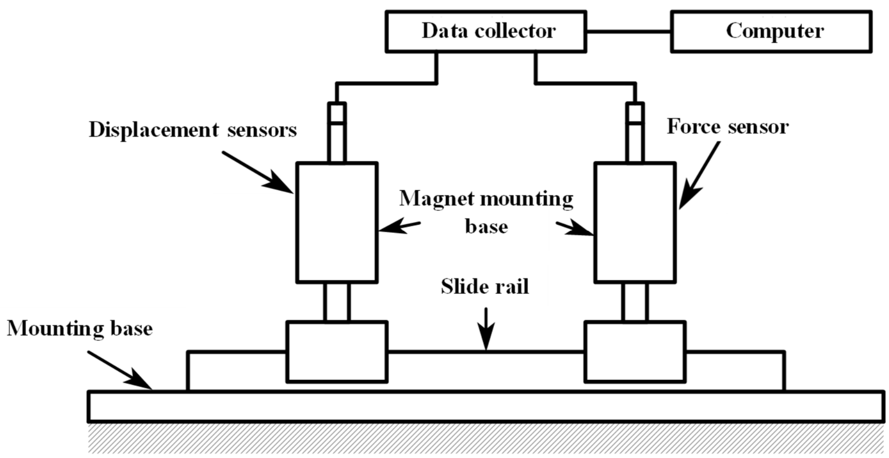

Figure 10. Schematic illustration of the magnetic force test system.

Various structural parameters of the magnetic attraction structure are shown in Table 1. The magnetic attraction structure is tested by using the testing mechanism of the magnetic force, and the magnetic force and displacement curves of the magnetic attraction structure in the range of 0–14 mm spacing are obtained. Figure 11 illustrates the COMSOL static magnetic field simulation results and the magnetic force test results. As can be seen, the displacement-magnetic force curve is obviously nonlinear, and the magnetic force increases with the increase of the displacement. Thereby, the magnetic stiffness is positively correlated with the displacement. Furthermore, it is clear that the experimental curve is in good agreement with the respective simulation curve, which verifies the accuracy of the simulated results. It is worth noting that the experimental curve lies upward compared with the simulation curve. This is due to the friction between the magnet sleeve and the magnet, resulting in errors during the measurements.

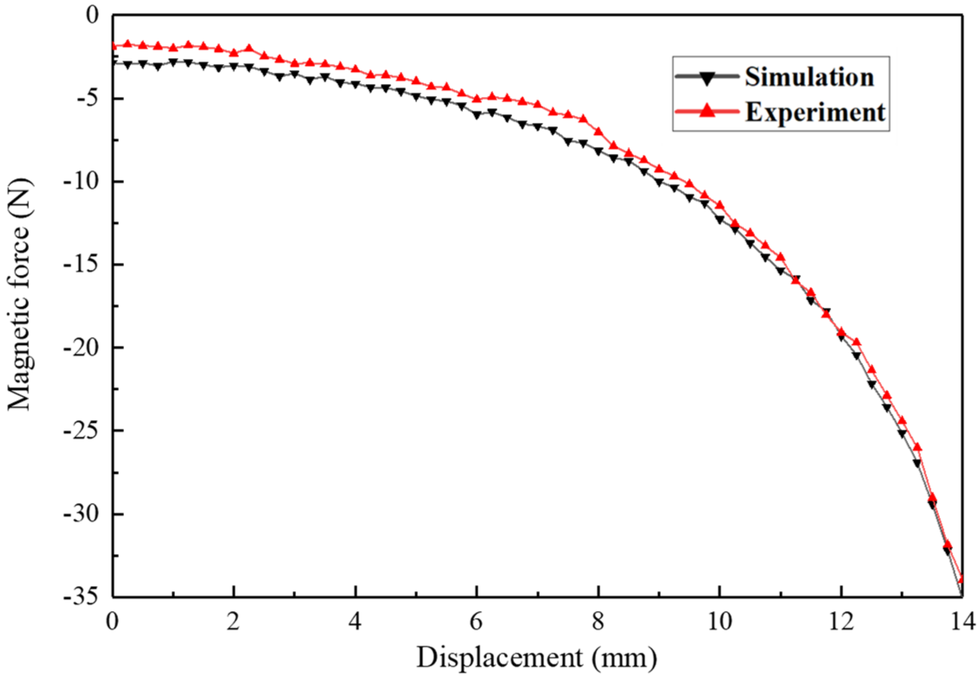

Figure 11. Comparison of the experimental and simulated outcomes.

4.2. Sound Absorption Test

The air sound standing wave tube method is used to test the sound absorption of the negative stiffness thin-film structure, and the test system is shown in Figure 12. Positions 1 and 2 refer to the interfaces of two acoustic sensors, respectively, where the right side is the specimen placement end, and the left side is the sound source. The impedance tube (AWA8551), signal generator (AWA6290M), and power amplifier (AWA5871) are also included. The sound absorption coefficient can be obtained by the following Equation (28):

$$\alpha = 1 - \left| \frac{G_{12} - G_I}{G_R - G_{12}} e^{j2kx_1} \right|^2 \tag{28}$$

where G_I is the transfer function of the incident sound wave, G_R is the transfer function of the reflected sound wave, G_{12} represents the transfer function, is the wave number, and k denotes the distance from the specimen surface to the interface 1.

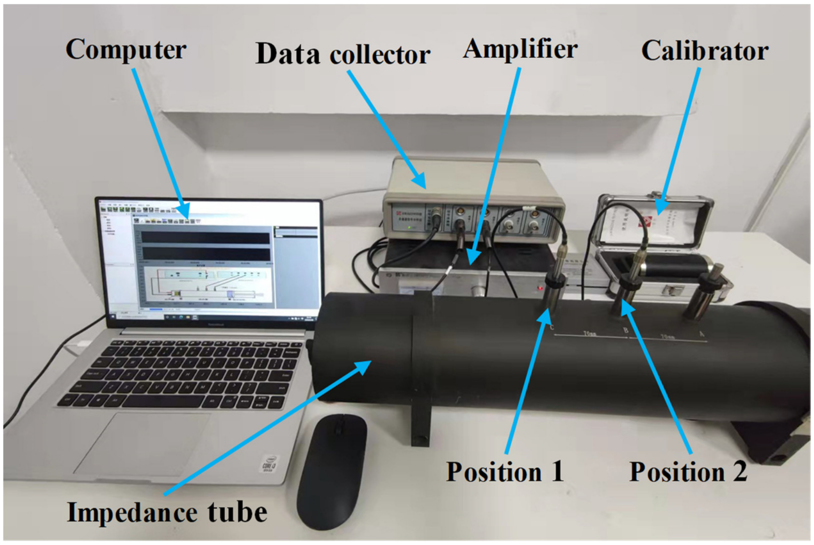

Figure 12. Sound absorption test system.

Firstly, the structural parameters of the film structure with negative stiffness are given. The thickness of the film is 0.2 mm, the distance between the mass and the permanent magnet is 10 mm, the depth of the back cavity is 50 mm, and the radius of the back cavity is 45 mm, while other parameters are shown in Table 1. The air acoustic standing wave tube sound absorption test system is used to test the sound absorption of the negative stiffness film structure. The coefficient curve of the sound absorption of the negative stiffness film structure in the frequency band of 100–1000 Hz is obtained. It is compared with theoretical analysis results, as is shown in Figure 13.

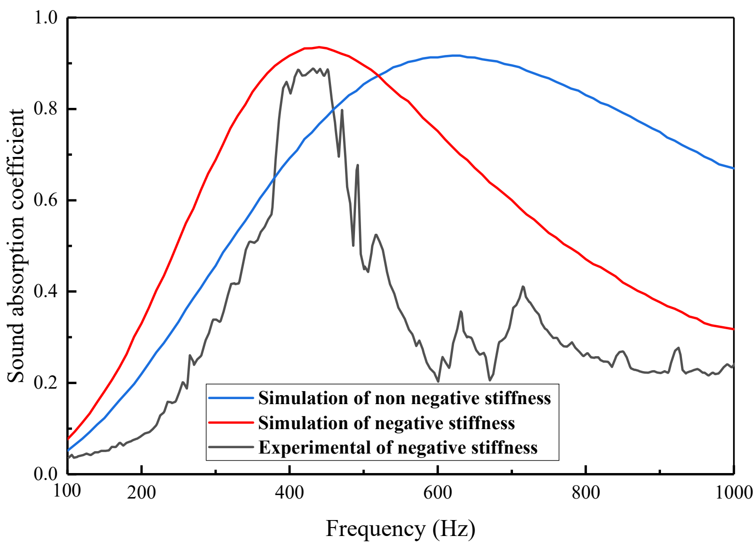

Figure 13. Comparison of the sound absorption experimental and simulated data.

Figure 13 shows the theoretical calculation of the sound absorption coefficient in the frequency range of 100–1000 Hz of the thin film mass cavity structure before and after adding the magnetic structure. As can be observed, after the magnetic structure is added, the frequency of the sound absorption peak is reduced from the original 620 Hz to 437 Hz, but the sound absorption band becomes narrower. Comparing the experimental curve with the calculated curve, it can be seen that the experimental curve will be moved downward as a whole compared with the theoretical curve, which indicates that the experimental data are smaller as a whole compared with the simulated data. This is mainly because the actual measurement process cannot form a perfect sound test environment, and a certain sound leakage phenomenon takes place. Besides, the external environment will also affect the test data. Nevertheless, the peak value of the experimental curve and the simulation fitting curve are in the same frequency band. They possess the same change trend, which verifies the accuracy of the proposed theoretical calculation.

5. Conclusions

In this work, a negative stiffness thin-film acoustic metamaterial model is established and verified by performing both simulations and experiments. Main conclusions that can be drawn as the following:

(1) The negative stiffness structure of the negative stiffness thin-film structure is analyzed, and the fitting relationship between the magnetic force and displacement is deduced through theoretical analysis. Based on the superposition principle of the series structure, the positive stiffness of the thin film and the negative stiffness of the magnetic force are combined, and the relationship between system stiffness and displacement is derived.

(2) Based on the finite element analysis method of the static magnetic field, the magnetic field finite element model of the magnetic structure is established, and the relationship between magnetic force and displacement of the magnetic structure is analyzed. Furthermore, the impact of the thickness of mass, the radius of mass, and the thickness of the permanent magnet on the magnetic force and magnetic stiffness are systematically studied.

(3) The solid mechanics model of thin-film is added to the magnetic structure, the magnetic-solid coupling simulation model is formed, and the relationship between system stiffness and displacement is given. The impacts of the change of the mass thickness, the radius, and the change of the film thickness on the system stiffness are studied.

(4) The magnetic force test platform of the negative stiffness thin-film structure is built and comparing the acquired experimental results with the respective finite element simulation results of the static magnetic field, a high degree of consistency is found. Results show that the proper addition of the magnetic suction structure can induce a shift of the absorption peak to a lower frequency region.

Author Contributions: X.Z.: Methodology, Formal analysis, Data curation, Investigation, Writing—Original draft. C.F.: Conceptualization, Methodology, Supervision, Writing—Review and editing. H.B.: Conceptualization, Methodology, Supervision, Writing—Review and editing. Z.L.: Supervision, Writing—Review and editing. X.L.: Conceptualization, Methodology, Supervision, Writing—Review and editing. All authors have read and agreed to the published version of the manuscript.

Funding: This research was funded by the financial support from the Education and Scientific Research Foundation for young teachers in Fujian Province, China (grant numbers JAT200034), the Natural Science Foundation of Fujian Province (Grant No. 2021J01130121) and the key technology project of Inner Mongolia (Grant No. 2021GG0437).

Data Availability Statement: The data presented in this study are available on request from the corresponding author. The data are not publicly available due to privacy.

Conflicts of Interest: The authors declare that they have no known competing financial interests or personal relationships that could have appeared to influence the work reported in this paper.

References

1. Zhou, R. *An Acoustic Metamaterial Based on Helmholtz Cavity and Membrane and Research on Transmission Loss in Low Frequency*; Jiangsu University: Zhenjiang, China, 2017.
2. Wen, J.H.; Wang, G.; Yu, D.L.; Zhao, H.G.; Liu, Y.Z.; Wen, X.S. Study on vibration band gap and damping characteristics of phononic crystals. *Sci. Sin.* **2007**, *37*, 1126–1139.
3. Cummer, S.A.; Christensen, J.; Alù, A. Controlling sound with acoustic metamaterials. *Nat. Rev. Mater.* **2016**, *1*, 16001. [CrossRef]
4. Li, J.; Chan, C.T. Double-negative acoustic metamaterial. *Phys. Rev. E Stat. Nonlinear Soft Matter Phys.* **2004**, *70*, 55602. [CrossRef]
5. Zuo, Y.Y.; Zhou, J.H.; Liu, H.B.; Hong, J.H. Sound absorptivity and application of perforated panel structure. *China Mech. Eng.* **2007**, *18*, 778–780.
6. Fan, Q.W.; Shen, Y.G.; Zhang, W. Analysis of interior sound field in Helmholtz resonant muffler. *Noise Control* **2007**, *31*, 67–69.

7. Ji, G.S.; Huber, J. Recent progress in acoustic metamaterials and active piezoelectric acoustic metamaterials—A review. *Appl. Mater. Today* **2021**, *26*, 101260. [CrossRef]
8. Chen, Z.X.; Peng, Y.H.; Li, H.X.; Liu, J.J. Efficient nonreciprocal mode transitions in spatiotemporally modulated acoustic metamaterials. *Sci. Adv.* **2021**, *7*, eabj1198. [CrossRef]
9. Sun, P.; Zhang, Z.d.; Guo, H.; Liu, N.N.; Jin, W.C.; Yuan, T.; Wang, Y.S. Topological optimization of hierarchical honeycomb acoustic metamaterials for low-frequency extreme broad band gaps. *Appl. Acoust.* **2022**, *188*, 108579. [CrossRef]
10. Yang, Z.; Mei, J.; Yang, M.; Chen, N.H.; Sheng, P. Membrane-type acoustic metamaterial with negative dynamic mass. *Phys. Rev. Lett.* **2008**, *101*, 204301. [CrossRef]
11. Naify, C.J.; Chang, C.M.; McKnight, G.; Nutt, S. Transmission loss and dynamic response of membrane-type locally resonant acoustic metamaterials. *J. Appl. Phys.* **2010**, *108*, 114905. [CrossRef]
12. Mei, J.; Ma, G.; Yang, M.; Yang, Z.Y.; Wen, W.J.; Sheng, P. Dark acoustic metamaterials as super absorbers for low-frequency sound. *Nat. Commun.* **2012**, *3*, 756–763. [CrossRef] [PubMed]
13. Fan, L.; Chen, Z.; Zhang, S.Y.; Li, X.J.; Zhang, H. An acoustic metamaterial composed of multi-layer membrane-coated perforated plates for low-frequency sound insulation. *Appl. Phys. Lett.* **2015**, *106*, 131–457. [CrossRef]
14. Chen, L.; Wu, W.G.; Zhou, R. A petal-like acoustic metamaterial structure based on local resonance with ultra-wide sonic band gap in low frequency range. *Tech. Acous.* **2016**, *35*, 222–227.
15. Gao, N.S.; Hou, H.; Mu, Y.H. Low frequency acoustic properties of bilayer membrane acoustic metamaterial with magnetic oscillator. *Theor. Appl. Mech. Lett.* **2017**, *7*, 252–257. [CrossRef]
16. Langfeldt, F.; Gleine, W.; Von, O. An efficient analytical model for baffled, multi-celled membrane-type acoustic metamaterial panels. *J. Sound Vib.* **2018**, *417*, 359–375. [CrossRef]
17. Sam, H.L.; Choon, M.P.; Yong, M.S.; Zhi, G.W.; Chul, K.K. Acoustic metamaterial with negative density. *Phys. Lett. A* **2009**, *373*, 4464–4469.
18. Kumar, S.; Bhushan, P.; Prakash, O.; Bhattacharya, S. Double negative acoustic metastructure for attenuation of acoustic emissions. *Appl. Phys. Lett.* **2018**, *112*, 101905. [CrossRef]
19. Yang, Z.; Dai, H.M.; Chan, N.H.; Ma, G.C.; Sheng, P. Acoustic metamaterial panels for sound attenuation in the 50–1000 Hz regime. *Appl. Phys. Lett.* **2010**, *96*, 041906. [CrossRef]
20. Shen, C.; Xie, Y.B.; Sui, N.; Wang, W.Q.; Cummer, S.A.; Jing, Y. Broadband acoustic hyperbolic metamaterial. *Phys. Rev. Lett.* **2015**, *115*, 254301. [CrossRef]
21. Christiansen, R.; Sigmund, O. Experimental validation of systematically designed acoustic hyperbolic meta material slab exhibiting negative refraction. *Appl. Phys. Lett.* **2016**, *109*, 101905. [CrossRef]
22. Gai, X.L.; Li, X.H.; Zhang, B.; Xie, P.; Ma, Z.H. Numerical simulation of sound-absorbing property of membrane materials. *Noice Vib. Control.* **2014**, *34*, 110–113.
23. Zhu, Q.; Bai, H.B.; Lu, C.H.; Huang, K.; Li, T. Study on the sound absorption property of a resonance-type material decorated with membrane. *Piezoelectr. Acoustoopt.* **2017**, *39*, 27–31.
24. Zhao, J.J.; Li, X.H.; Wang, Y.Y.; Wang, W.J.; Zhu, L.; Zhang, B. Low frequency sound absorption of a menbrane-type with magnetic negative stiffness. *Acta Acust.* **2017**, *42*, 239–245.
25. Qian, W.C.; Wang, Z.Z.; Xu, Y.G.; Chen, S.L. Symmetrical deformation of the central part of a circular film under uniformly distributed load. *Appl. Math. Mech.* **1981**, *6*, 599–612.